

# Wind flow characteristics and their loading effects on flat roofs of low-rise buildings

Zhongshan Zhao<sup>†</sup>

*Mustang Engineering Inc., 16001 Park Ten Place, Houston, TX 77084, USA*

Partha P. Sarkar<sup>‡</sup>

*Department of Aerospace Engineering and Engineering Mechanics, Iowa State University, Ames, IA 50011-2271, USA*

Kishor C. Mehta<sup>‡†</sup>

*Wind Engineering Research Center (WERC), Department of Civil Engineering, Texas Tech University, Lubbock, TX 79409-1023, USA*

Fuqiang Wu<sup>‡‡</sup>

*ABS Consulting, 16850 Diana Lane, Houston, TX 77058-2527, USA*

**Abstract.** Wind flow and pressure on the roof of the Texas Tech Experimental Building are studied along with the incident wind in an effort to understand the wind-structure interaction and the mechanisms of roof pressure generation. Two distinct flow phenomena, cornering vortices and separation bubble, are investigated. It is found for the cornering vortices that the incident wind angle that favors formation of strong vortices is bounded in a range of approximately 50 degrees symmetrical about the roof-corner bisector. Peak pressures on the roof corner are produced by wind gusts approaching at wind angles conducive to strong vortex formation. A simple analytical model is established to predict fluctuating pressure coefficients on the leading roof corner from the knowledge of the mean pressure coefficients and the incident wind. For the separation bubble situation, the mean structure of the separation bubble is established. The role of incident wind turbulence in pressure-generation mechanisms for the two flow phenomena is better understood.

**Key words:** flat-roofed low-rise buildings; wind loading effects; cornering vortices; separation bubble; incident wind-structure interaction; peak pressure generation mechanisms; pressure prediction model.

---

## 1. Introduction

Post-disaster surveys of building damage caused by severe winds have repeatedly revealed the

<sup>†</sup> Senior Structural Specialist

<sup>‡</sup> Associate Professor and Wilson Chair, Director

<sup>‡†</sup> P.W. Horn Professor and Director

<sup>‡‡</sup> Project Engineer

vulnerability of low-rise building roofs. Peak-pressure coefficients in the order of  $-25$  have been recorded on the roof of the Texas Tech Experimental Building. A brief description of this Experimental Building will be given in the next section. Over the flat roof of a rectangular low-rise building, two flow phenomena are identified. They are the cornering or conical vortices and the separation bubble. The conical vortices are generated over the leading roof corner at oblique incident wind. The separation bubble forms at wind perpendicular to the front wall when up-wash airflow above the stagnation point on the front wall separates at the roof edge. Available literature in wind engineering focuses mostly on the cornering vortices and their loading effects. Notwithstanding the significant practical importance in wind-load design, our efforts to predict the peak loads have been the least successful with the roof-corner region. Recent studies by Tieleman *et al.* (1994), Kawaii and Nishimura (1996), Marwood (1996) and Banks *et al.* (1997) attempt to refine the understanding of the cornering vortex phenomenon over the roof and the pressures induced on the underlying roof surface. One salient feature of the point-pressure under the separation bubble observed in full-scale tests is the short duration of peak pressures. The pressure generating mechanisms of the two phenomena have not been fully understood. Full-scale studies of the incident wind and its relationship with the cornering vortices and the pressure could uniquely contribute to a better understanding of the wind's loading effects on low-rise buildings. This paper discusses the fundamentals of the cornering vortices and separation bubble. It emphasizes the interaction of the incident wind, the near-surface flow characteristics and the pressure on the building roof, based on a full-scale study on the Texas Tech Experimental Building.

## 2. Facility and experimental setup

The Texas Tech Experimental Building, also known as the WERFL (Wind Engineering Research Field Laboratory) facility is a rectangular, flat-roofed low-rise building with a dimension of  $9.1$  (B)  $\times$   $13.7$  (L)  $\times$   $4.0$  (H) m ( $30 \times 45 \times 13$  ft). In this section, the location and coordinates of the relevant pressure

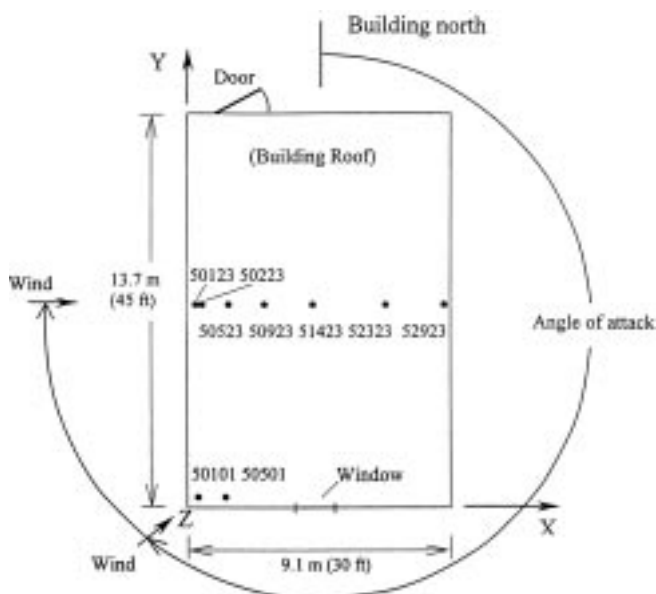


Fig. 1 Definition of wind angle of attack, tap location and coordinate system

taps on the roof are defined. These taps are 50101, 50501, 50123, 50223, 50523, 50923, 51423, 52323 and 52923.

Fig. 1 indicates the location of the taps on the building roof, the coordinate axes, the building north and the definition of wind angle of attack (AOA). The coordinates of the taps are specified in Table 1.

A 49 m (160 ft) high meteorological tower equipped with propeller-type UVW three-component anemometers is part of the facility to document the near-ground wind at six levels. It is located at a distance of 46 m (150 ft) southwest of the building such that it measures the predominant southwest winds in the area with minimized disturbance from the Experimental Building itself.

In addition to the UVW anemometers on the meteorological tower, sonic anemometers were also used in this study. Sonic anemometers were selected for their fast frequency response and their capability to accurately detect wind flow direction, a feature essential to the measurement of highly turbulent flow over the building roof. The spatial resolution of the sonic anemometers is comparable to that of the hot-wire probes used on scaled low-rise building models (typical scales are 1:50~1:100) in the

Table 1 Coordinates of relevant pressure taps on the roof

Tap	Coordinates		Location
	$x$ m (ft)	$y$ m (ft)	
50123	0.30 (1.00)	7.06 (23.17)	Short axis
50223	0.51 (1.67)	7.06 (23.17)	Short axis
50523	1.42 (4.67)	7.06 (23.17)	Short axis
50923	2.64 (8.67)	7.06 (23.17)	Short axis
51423	4.32 (14.18)	7.06 (23.17)	Short axis
52323	6.88 (22.58)	7.06 (23.17)	Short axis
52923	8.91 (29.25)	7.06 (23.17)	Short axis
50101	0.36 (1.2)	0.36 (1.2)	Roof corner
50501	1.42 (4.67)	0.36 (1.2)	Roof corner

Note:  $x$  and  $y$  are defined in Fig. 1



Fig. 2 Sonic anemometer setup on the roof

wind tunnel. The sonic anemometers (Model 1210K-063, Gill Instruments Ltd., Fig. 2) can measure wind speed at rates up to 100 Hz (full 3-axis measurement). It samples an air volume of about  $850 \text{ cm}^3$  ( $52 \text{ in}^3$ ), i.e., a cylinder with a diameter of 10.2 cm (4 in.) and a height of 10.5 cm (4.13 in.), enclosed by three pairs of probes. The flight distance between each pair of probes is 14.6 cm (5.75 in.). The anemometer measures three axial velocities, which are converted into three orthogonal velocity components. The sonic anemometers were used for measuring the incident wind as well as the flow inside the separation bubble.

### 3. Incident wind characteristics

The wind speed and direction of natural wind changes constantly in time and space. The study of wind-building interaction requires knowledge of the characteristics of the incident wind as it approaches the building. It was assumed that the measurement of incident wind at the meteorological tower, 49 m (160 ft) away from the building, with propeller-type UVW anemometers may not be adequate. To overcome this deficiency, one sonic anemometer with much faster frequency response was placed in the vicinity of the building to measure the incident wind speed and direction as it approached the building. Besides the frequency-response concern, it needed to be verified that the wind measured with the sonic anemometer placed near the building actually represents the undisturbed upstream wind. For verification and comparison, two sonic anemometers, one mounted on a portable pole close to the tower and one located close to the building, and one UVW anemometer on the meteorological tower were used; it must be considered that wind characteristics will change in the time domain after the wind travels a distance of 49 m (160 ft) from the tower to the test building.

#### 3.1. Upstream wind: UVW measurement on meteorological tower

The wind speed and the wind direction measured at the meteorological tower using UVW anemometers are not used directly to investigate the relationships between the incident wind, wind flows over the roof and pressure on the roof. They are instead used for comparisons and verification of the upstream wind measured by the UVW and sonic anemometers placed at different locations with respect to the building.

#### 3.2. Upstream wind: sonic measurements

All data runs of simultaneous sonic/UVW anemometer and pressure measurements were 15 minutes in duration. The sampling frequency for the sonic anemometers and the pressure was 30 Hz, while that for the UVW anemometer was 10 Hz. Two sonic anemometers were employed in order to compare the incident winds measured at the tower and at a location much closer to the building. Sonic anemometer #1 was mounted on a movable pole at the elevation of 4 m (13 ft) such that the separation between the sonic and UVW anemometers mounted on the tower at the same elevation was 1.8 m (6 ft); sonic anemometer #2 was located close to the building. In the case of cornering vortices, sonic anemometer #2 was fixed at about 1.5 m (5 ft) above the leading roof corner; this clearance was considered sufficient for the sonic anemometer to stay outside of any vortical circulation. In the separation bubble case, sonic anemometer #2 was placed above the leading roof edge at varying heights (greater than 40 cm or 16 inches) for different data runs.

### 3.3. Comparison of incident wind between sonic and UVW measurements

Statistical comparisons of incident wind are made between sonic anemometers #1 and #2, and between sonic anemometers #1 and #2 and the UVW anemometer. The side-by-side placement of sonic anemometer #1 and the UVW anemometer was done to ensure that the wind passing through the two anemometers was very similar, and any discrepancies could be attributed to differences in the two instruments.

Table 2 compares the longitudinal incident wind speed and wind direction between the UVW anemometer at the tower and the sonic anemometer #2 above the building edge for the separation bubble case. It is worth mentioning that the correction factors in Table 2 are specific to the locations of the sonic anemometer. The comparisons of mean and rms values for the wind speed and the

Table 2 Two-way comparisons of mean wind speed and mean wind azimuth: UVW anemometer and sonic anemometer #2

–	UVW on tower ( 4 m level )						Sonic #2	
	Wind azimuth (°)			Wind speed, m/s			AOA (°)	Correction factor*
Run No.	mean	rms	range	mean	rms	mean/rms	mean/rms	–
M49n50	0.6	10.1	61	8.18	1.50	255.6/10.1	258.5/16.7	1.07
M49n72	142.7	8.8	118	6.39	1.47	262.7/8.8	260.8/13.9	1.15
M49n105	230.6	10.95	70	8.18	1.82	275.6/10.9	279.6/16.8	0.97
M49n145	30.8	11.75	87	9.48	1.32	270.8/11.7	271.0/15.5	1.08
M49n213	233.8	10.8	87	13.59	2.20	263.8/10.8	265.4/12.9	1.07

\*This factor is the ratio of the mean wind speed measured by the sonic anemometer #2 near the building to that measured by the UVW anemometer at the meteorological tower; it was used to correct the time histories of sonic # 2 measurements to recover the undisturbed incident wind.

Table 3 Three-way comparisons of mean wind speed and mean wind azimuth

Run No.	UVW at Tower 4 m				Sonic #1 at Tower 4 m				Sonic #2 at Roof Corner			
	Long.	Lat.	Vert.	Azim.	Long.	Lat.	Vert.	Azim.	Long.	Lat.	Vert.	Azim.
M52n069	6.22	0.00	0.04	265.34	6.48	0.00	0.11	264.48	6.90	0.00	0.75	263.63
M52n070	6.98	0.00	0.02	270.38	7.27	0.00	0.09	269.67	7.38	0.00	0.83	269.47
M52n071	7.14	0.00	0.02	274.15	7.41	0.00	0.09	273.69	7.65	0.00	0.91	273.85
M52n072	7.59	0.00	0.06	275.47	8.87	0.00	0.11	275.16	8.03	0.00	1.01	275.39
M52n073	8.33	0.00	0.01	275.27	8.64	0.01	0.09	275.06	8.61	0.01	1.02	275.50
M52n074	8.82	0.00	0.00	269.53	9.12	0.01	0.10	268.92	9.36	0.01	1.08	270.00
M52n075	9.06	0.00	0.04	269.28	9.42	0.00	0.12	268.73	9.83	0.00	1.12	268.27
M52n076	8.26	0.00	0.06	266.34	8.59	0.00	0.10	265.51	8.83	0.00	1.03	265.06
M52n077	8.72	0.01	0.06	262.92	9.08	0.01	0.13	262.14	9.30	0.01	0.98	261.29
M52n078	8.27	0.00	0.06	265.51	8.58	0.00	0.12	264.78	8.90	-0.01	1.05	264.49

Note: Wind speeds are in m/s; azimuth angle is in degrees

Long. = Longitudinal wind speed ( $u$ )

Lat. = Lateral wind speed ( $v$ )

Vert. = Vertical wind speed ( $w$ )

Azim. = Azimuth angle, measured from true north

Table 4 Three-way comparisons of turbulence intensities ( $I_u$ ,  $I_v$  and  $I_w$ )

Run No.	UVW at Tower 4 m			Sonic #1 at Tower 4 m			Sonic #2 at Roof Corner		
	$I_u$	$I_v$	$I_w$	$I_u$	$I_v$	$I_w$	$I_u$	$I_v$	$I_w$
M52n069	0.184	0.133	0.055	0.199	0.161	0.096	0.171	0.174	0.094
M52n070	0.224	0.150	0.057	0.230	0.179	0.095	0.230	0.193	0.098
M52n071	0.233	0.149	0.061	0.240	0.177	0.095	0.213	0.188	0.097
M52n072	0.216	0.185	0.059	0.228	0.210	0.093	0.230	0.227	0.097
M52n073	0.216	0.214	0.056	0.229	0.242	0.093	0.232	0.272	0.099
M52n074	0.206	0.165	0.058	0.214	0.190	0.094	0.211	0.201	0.096
M52n075	0.211	0.155	0.061	0.222	0.182	0.094	0.198	0.190	0.094
M52n076	0.218	0.170	0.062	0.225	0.193	0.098	0.228	0.213	0.099
M52n077	0.214	0.201	0.053	0.225	0.218	0.091	0.199	0.234	0.090
M52n078	0.207	0.186	0.062	0.219	0.209	0.094	0.182	0.231	0.096

Note:  $I_u$  = Turbulence intensity of the longitudinal component

$I_v$  = Turbulence intensity of the lateral component

$I_w$  = Turbulence intensity of the vertical component

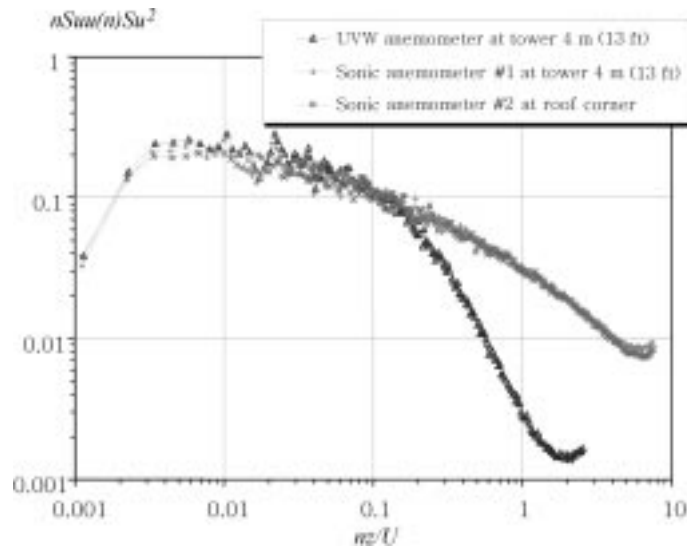


Fig. 3 Comparison of spectrum: longitudinal wind speed component ( $u$ )

azimuth angle are favorable, considering possible misalignment of the instruments. The correction factors are consistently greater than 1.0 with the exception of one value because the wind flow above the roof edge is accelerated. More detailed three-way comparisons of incident-wind measurements are given in Tables 3 and 4. The comparisons are very satisfactory except the vertical component, as expected. The spectra of the three wind speed components ( $u$ ,  $v$  and  $w$ ) from the three different anemometers are compared in Figs. 3, 4 and 5. From these figures, it is apparent that the propeller-type UVW anemometer is deficient in high-frequency response. The spectra of the longitudinal component ( $u$ , Fig. 3) from the two sonic anemometers are very similar, while small differences do exist for the lateral ( $v$ , Fig. 4) and the vertical ( $w$ , Fig. 5) components. It is concluded from these

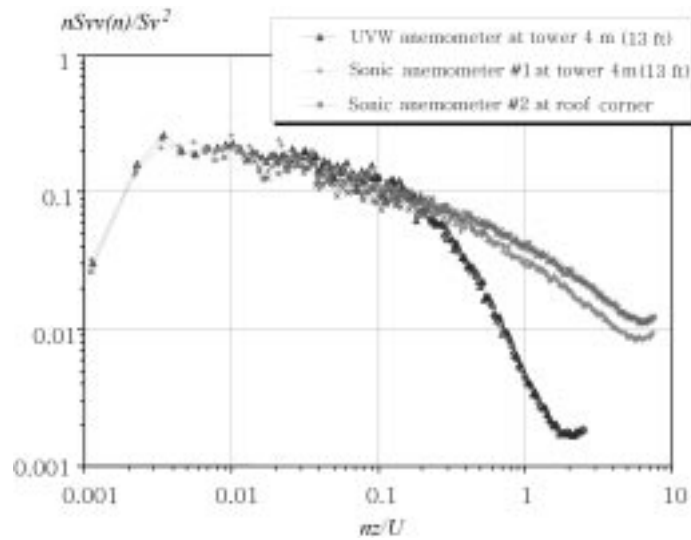


Fig. 4 Comparison of spectrum: lateral wind speed component ( $v$ )

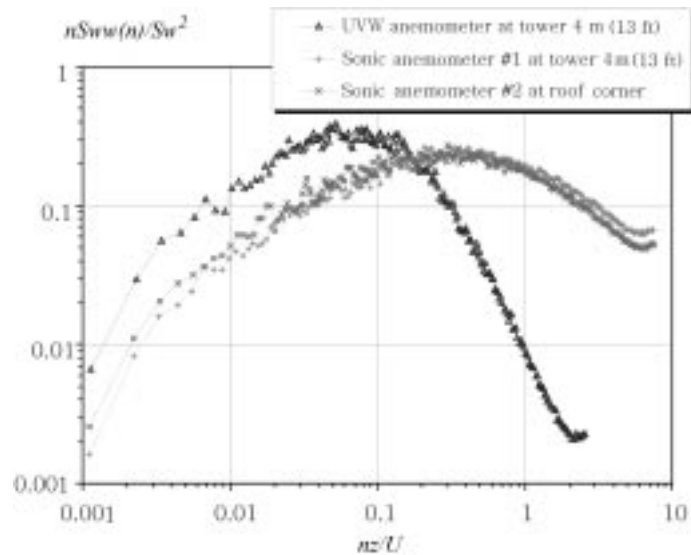


Fig. 5 Comparison of spectrum: vertical wind speed component ( $w$ )

comparisons that the sonic anemometer measurement of the incident wind, at a properly chosen location close to the building, can satisfactorily represent the upstream wind conditions.

#### 4. Cornering vortices

In this section of the paper, the mean pressure coefficients for roof-corner taps 50101 and 50501 are first examined in terms of their relationship with the mean wind angle-of-attack (AOA). Flow visualization, together with synchronized measurements of the incident wind speed, wind direction

and the roof corner pressure, is conducted using the grid-tuft technique (Sarkar *et al.* 1997) over the leading roof corner to understand the characteristics of the cornering vortices and the mechanism of pressure generation. The incident wind used hereafter was measured by sonic anemometer #2. A simple mathematical model is then proposed for predicting the fluctuating pressures. The prediction model makes use of the incident wind speed and direction, and a pressure coefficient-incident wind angle relationship, which in this study is a curve-fitted functional relationship between the mean pressure coefficient and the mean wind angle.

#### 4.1. Pressure coefficients on roof corner under cornering vortices

The study of the conical vortices focuses on two roof-corner pressure taps, i.e., 50101 and 50501,

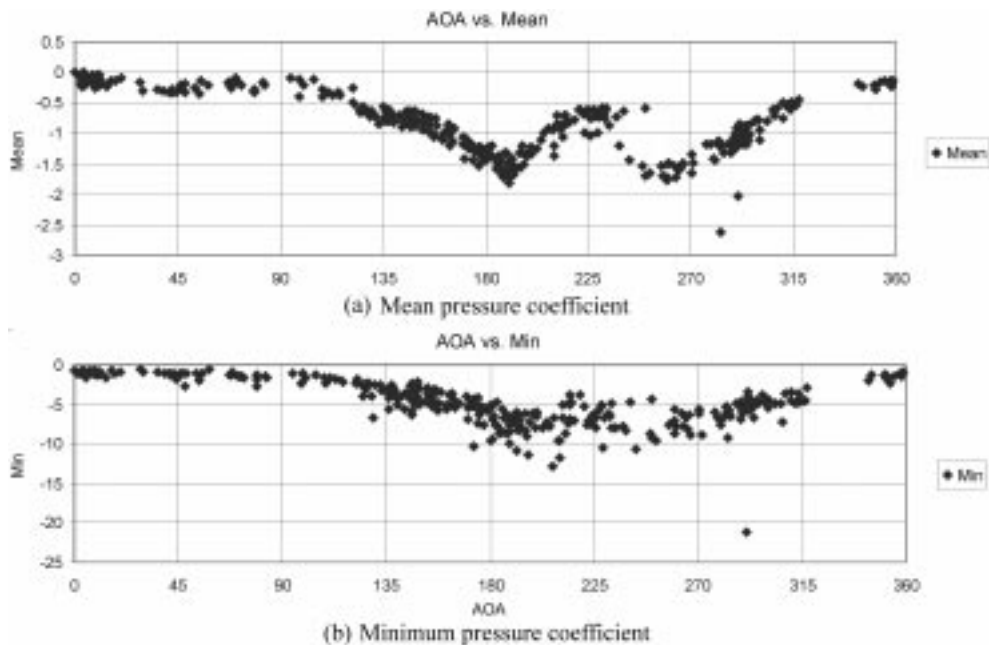


Fig. 6 Pressure coefficients (tap 50101) versus wind angle of attack

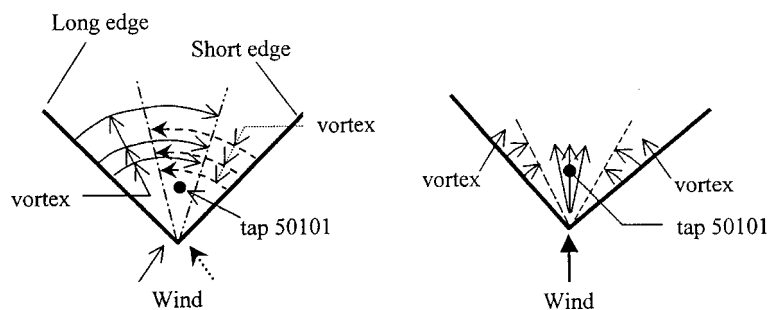


Fig. 7 Schematics of cornering vortices and location of tap 50101

to examine the incident wind angle-pressure coefficient relationship. The location of the two taps and their coordinates are shown in Fig. 1 and Table 1, respectively. The mean and the minimum pressure coefficients of tap 50101 versus the incident wind angle of attack are shown in Fig. 6. In Fig. 6(a), the mean pressure coefficient has two peaks at about  $190^\circ$  and  $260^\circ$  AOA, respectively, and a much-reduced (less negative) pressure occurs at wind AOA around  $225^\circ$ . It is understood that high suction on the leading roof corner are a direct result of strong vortical circulation. The two peaks are due to the fact that tap 50101 is located on the bisector of the roof corner. Tap 50101 is therefore beneath either the vortex generated at the long roof edge with a wind AOA of about  $260^\circ$ , or the vortex formed at the short roof edge with a wind AOA around  $190^\circ$ . At wind AOA around  $225^\circ$ , as will be shown later, two small vortices are generated, but neither vortical circulation is big enough to be directly over tap 50101; the wind flow that passes over this tap is mostly non-vortical, resulting in a significant reduction in the pressure at the tap. This is schematically shown in Fig. 7.

A similar argument can be made about pressure tap 50501, except that tap 50501 is close to the short roof edge and is usually under the influence of only the vortex formed from flow separation at that edge. As a result, the mean pressure coefficient of tap 50501 has only one peak at wind AOA of  $200^\circ$ ~ $210^\circ$ . Fig. 8 gives the pressure coefficient-wind AOA relationship for tap 50501. Similar information about a few other taps can be found in Zhao (1997). The data in Figs. 6 and 8 were collected over a period of 18 months from April 1991 through September 1992, representing about 350 15-minute data runs; the averaged mean wind speed for these data runs is 22 mph at 33 ft, and the averaged longitudinal turbulence intensity is 0.18 with a range of 0.12 through 0.39.

In Figs. 6 and 8, a run-averaged wind angle was used. The use of the run-averaged wind angle is convenient and acceptable when the mean pressure coefficients are dealt with. However, it is not

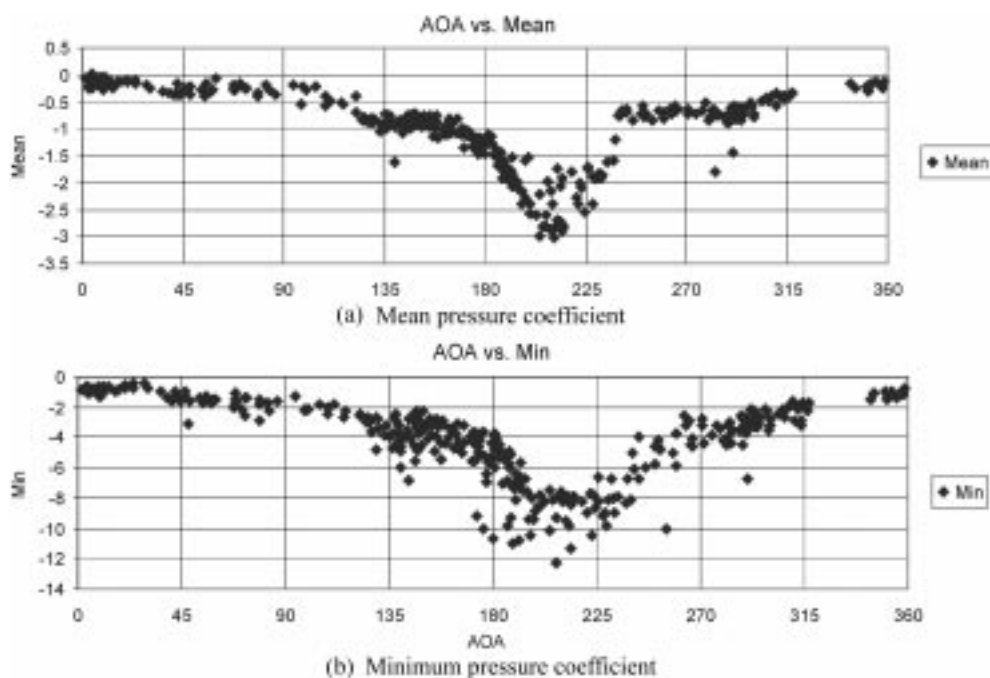


Fig. 8 Pressure coefficients (tap 50501) versus wind angle of attack

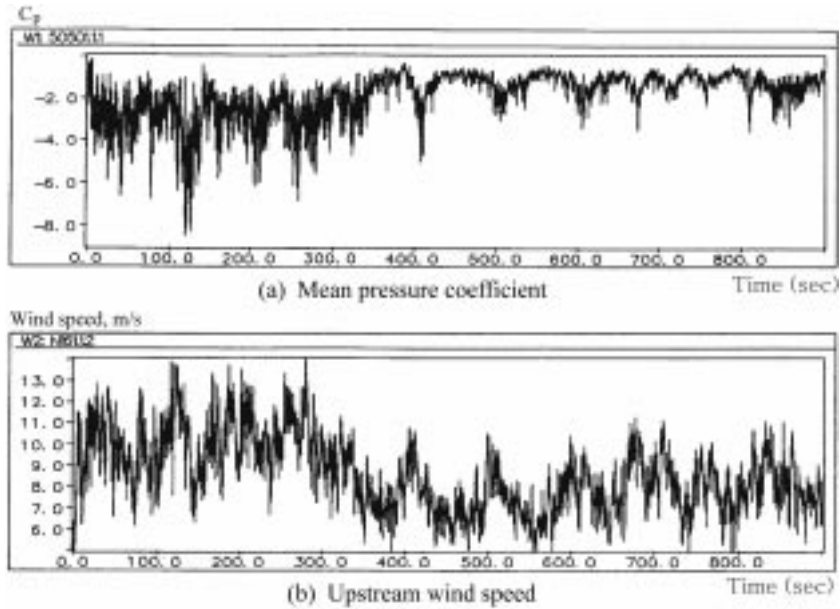


Fig. 9 Simultaneous traces of upstream wind speed and pressure coefficient (tap 50501)

always consistent to use the run-averaged wind angle in the case of the minimum pressure coefficient, since the minimum value is a single data point in a time series. In most situations, the minimum pressure coefficient occurs at an incident wind angle that is different from that of the run-averaged wind angle. According to the definition of pressure coefficient, using run-averaged wind speed, the minimum pressure coefficient at an instant  $t$  is not unique, although the pressure at  $t$  is. The mean wind speed changes with the interval and starting time of the period over which the averaging is applied. This inconsistency may be partly responsible for the scatter in the distribution of the minimum pressure coefficient in Figs. 6(b) and 8(b). The minimum pressure coefficient in Fig. 6(b) would have had less scatter and two distinct peaks, as was the case with the corresponding mean pressure coefficient in Fig. 6(a), had the instantaneous wind angle been used instead of the run-averaged wind angle. This is verified indirectly through the successful prediction of the fluctuating pressure coefficient in Section 4.3.

Moreover, it is observed that the fluctuations of the pressure on the leading roof corner closely respond to the changes in the incident wind speed. This trend is visible in Fig. 9. In the past, Letchford *et al.* (1993) and Hoxey and Short (1999) have emphasized the effect of wind speed on pressures in the context of quasi-steady theory.

#### 4.2. Flow visualization and features of cornering vortices

Flow visualization experiments using the tuft-grid method were designed to understand the fundamentals of the cornering vortices at skewed incident winds. By systematically moving the grid (placed perpendicular to the long roof edge) to desired locations, the core position of the vortex forming at that edge could be determined. The grid was oriented perpendicular to the roof-corner bisector to visualize the vortex pair.

#### 4.2.1. Position of vortex core

The cornering vortex core forms a continuous three-dimensional curve that can be approximated by a series of discrete points obtained in flow visualization. These discrete points are specified by their coordinates  $(x, y, z)$ , which were defined in Fig. 1. Coordinates  $x$ ,  $y$ , and  $z$  obey the right-hand rule, with the origin at the roof corner. Coordinate  $y$  is the distance along the long roof-edge; it denotes the location of the visualization grid;  $x$  is the distance along the short roof-edge, i.e., the offset of the vortex core from the long roof edge;  $z$  is the vertical displacement of the vortex core from the roof surface. Table 5 summarizes the vortex core coordinates, at the incident wind along the roof-corner bisector. The same data are displayed graphically in Fig. 10. It can be seen that a straight line approximates quite well the change of the core displacement ( $z$ ) with  $y$ , the distance measured along the long edge. For the offset ( $x$ ) of the vortex core from the long roof edge, a linear curve fitting with  $y$  is acceptable up to about  $y = 3.7$  m (12 ft), while a curve of the second order might be a better approximation up to  $y = 6.1$  m (20 ft). It must be pointed out that the core position readings from the visualization are best estimates. Fig. 10 indicates that the vortex-core displacement rises at a slope of 7.25% and the vortex core has an initial displacement of 1.5 cm at  $x = 0$ . Close to the roof corner, the projection of the vortex core on the roof takes an angle of about  $10^\circ$  with the long roof edge.

Banks *et al.* (2000) performed flow visualization on cuboidal models (45 cm to 120 cm) in wind-tunnel generated non-boundary-layer turbulent flows. In their experiments, glycerin smoke was introduced through holes near the leading roof corner, and a laser-light sheet perpendicular to one of the roof edges was used to visualize the vortex. It was found that at  $225^\circ$  wind angle of attack the

Table 5 Vortex-core positions at wind angle of attack of  $225^\circ$

Run #	Grid location ( $y$ ), m	Offset ( $x$ ), m	Displacement ( $z$ ), m	Mean wind speed, m/s
M49n160	1.96	0.30	0.15	8.9
M49n169	2.62	0.46	0.23	8.5
M49n158	3.35	0.53	0.23	8.9
M49n168	3.78	0.61	0.30	8.9
M49n161	4.70	0.69	0.38	7.2
M49n167	5.66	0.76	0.38	8.9
M49n162	5.99	0.76	0.46	7.6

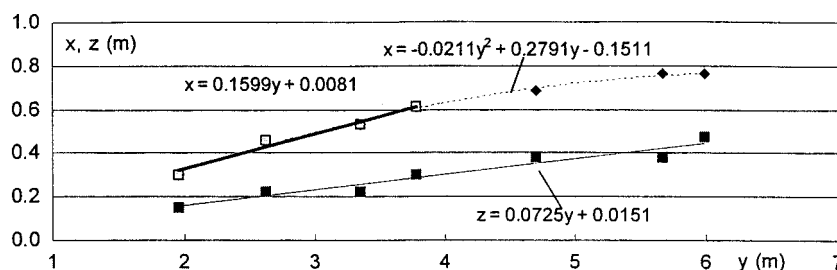


Fig. 10 Position of vortex core derived from flow visualization

vortex core has an initial displacement of 2 mm (the full-scale equivalent is about 1.7 cm) above the roof corner and it rises at a slope of 7%; the vortex core projection in the horizontal plane assumes an angle of  $12^\circ$  with the roof edge. These values are comparable with the results of the current study.

#### 4.2.2. Form and pattern of vortex pair

Based on the observations through flow visualization, the shape of vortex and the pattern of the vortex pair are established. In general, depending on the incident wind angle, the two vortices change in size and shape, and the vortex pair has a variety of patterns. Here, the wind angle of concern is in the range of  $180^\circ\sim 270^\circ$ .

A single vortex is first examined. The grid was set perpendicular to the long roof edge to visualize the vortex forming from flow separation at that edge. Fig. 11 shows the vortex formed at a wind

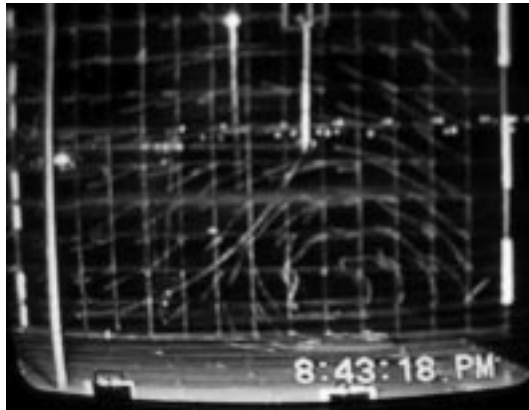


Fig. 11 Vortex formed at long roof edge at  $y = 1.83$  m (6 ft),  $AOA=210^\circ$ , M49n160

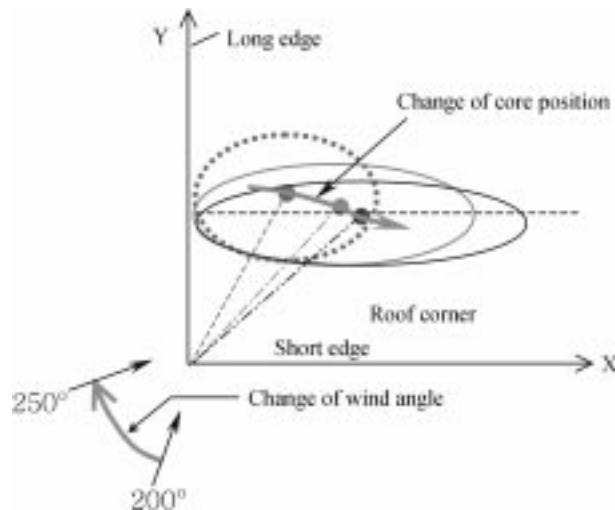


Fig. 12 Effect of wind angle of attack one vortex shape and core position

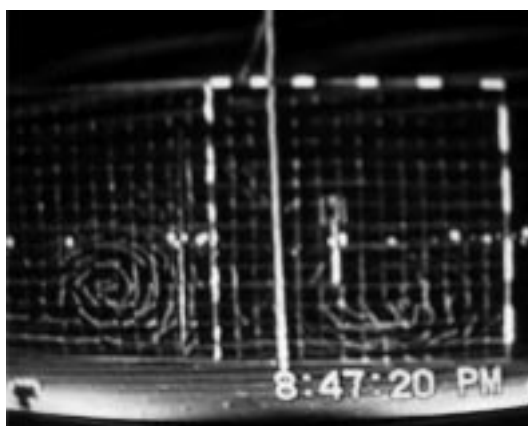


Fig. 13 Vortex pair formed at  $AOA=230^{\circ}\sim 235^{\circ}$

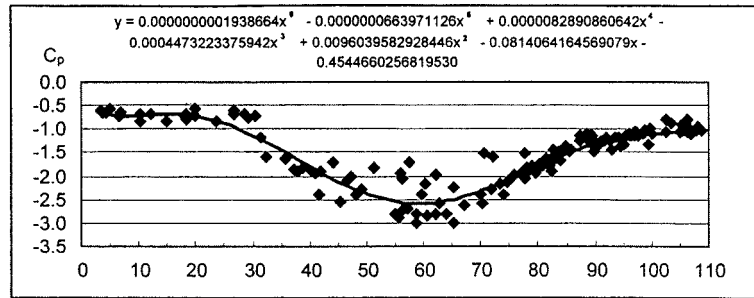
angle of about  $210^{\circ}$ ; the camera was placed on the downstream side of the grid. The vortex is observed to change in shape and location with the fluctuation of the incident wind angle. At larger wind angles, the vortex formed at the same edge is more oblong, and its core has a larger horizontal offset and a smaller displacement from the roof surface. This is conceptually generalized and depicted in Fig. 12.

At a certain range of wind angles around  $225^{\circ}$ , a pair of vortices forms. To visualize the vortex pair, the grid is oriented perpendicular to the roof-corner bisector, and the camera was set on the downstream side of the grid. Fig. 13 captures one of those instants when a pair of vortices is formed. The wind angle is in the range of  $230^{\circ}\sim 235^{\circ}$  at that particular instant.

#### 4.3. A model for pressure prediction

It was observed previously that both the incident wind speed and the incident wind angle are important factors governing the pressure generation on the leading roof corner at an oblique wind; the mean pressure coefficient-mean wind angle relationships presented in Figs. 6 and 8 indicate the importance of the wind angle. A typical plot of simultaneously varying wind speed and pressure (as in Fig. 9) hints at the possibility that there is a direct influence of the dynamic wind speed on pressures. Inspired by those observations, a numerical model is proposed to predict the fluctuating pressure coefficients from a relationship between the pressure coefficient and the incident wind; the relationship between the mean pressure coefficient and the mean wind angle obtained in the full-scale experiment can be used as an acceptable approximation. This relationship represents one of the fundamental properties of the cornering vortices, i.e., the characteristics of roof-corner vortices, thus the pressure coefficients on the roof surface under the vortices are closely related to the incident wind angle.

Using a simple mathematical model, the time-varying pressure coefficient for tap 50501 is created from the incident wind data of run M49n158. The functional relationship between the mean pressure coefficient and the mean wind angle for tap 50501 used in the model is shown in Fig. 14. Here a different definition of the wind angle is adopted. The wind angle perpendicular to the long roof edge is defined as  $0^{\circ}$ , and the wind angle perpendicular to the short edge is defined as  $90^{\circ}$ . The data points in Fig. 14 cover a wind angle range of  $\alpha=3.3^{\circ}\sim 108.7^{\circ}$  and are curve-fitted to a polynomial to



Note:  $x = \alpha$ ,  $y = C_p(\alpha)$ .

Wind angle ( $\alpha$ )

Fig. 14 Mean pressure coefficient versus wind angle (tap 50501)

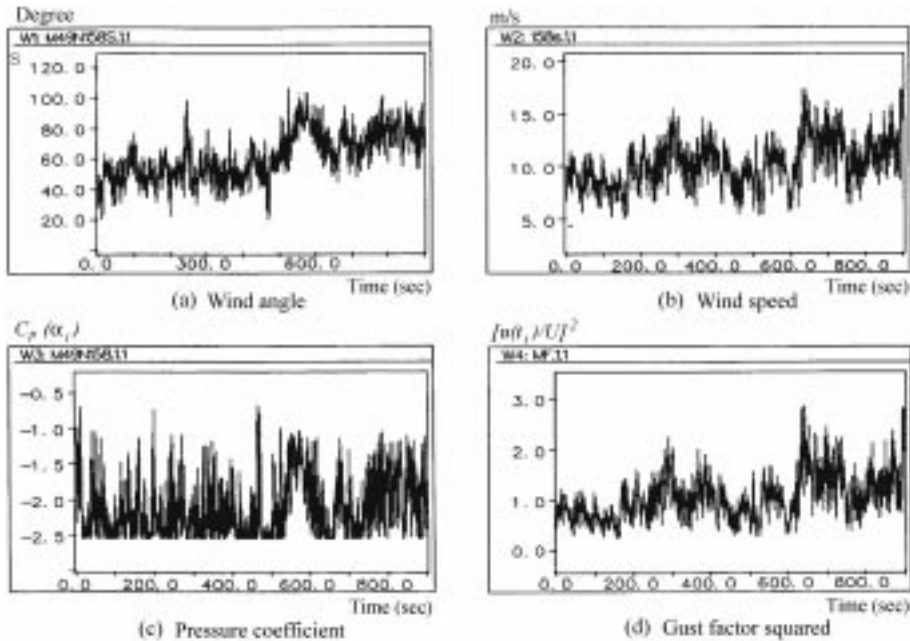


Fig. 15 Traces of variables used in pressure prediction (M49n158)

establish  $C_p(\alpha)$ . The higher order terms and long decimals in the curve-fitting in Fig. 14, where  $y$  is the  $C_p$  and  $x$  is the mean wind angle in degrees, are necessary for precision, if only one equation is used for the entire range of wind angle of interest; lower order polynomials can be satisfactory for piece-wise curve-fitting. This function is used to obtain the instantaneous  $C_p(\alpha_i)$  from the time series of the measured wind angle ( $\alpha_i$  at time  $t_i$ ), by sonic anemometer #2 placed close to the building, to calculate the instantaneous  $C_p(t_i)$ , using formula  $C_p(t_i) = C_p(\alpha_i) \times [u(t_i) / U]^2$ , where  $u(t_i)$  is the measured incident wind speed, and  $U$  is the run-averaged wind speed, both measured with sonic anemometer #2 located at about 1.5 m (5 ft) above the roof corner.

Example traces of the variables used in the above computation are illustrated in Fig. 15. Fig. 15(a) is the instantaneous incident wind angle ( $\alpha_i$ ); Fig. 15(b) shows the wind speed,  $u(t_i)$ ; Fig. 15(c)

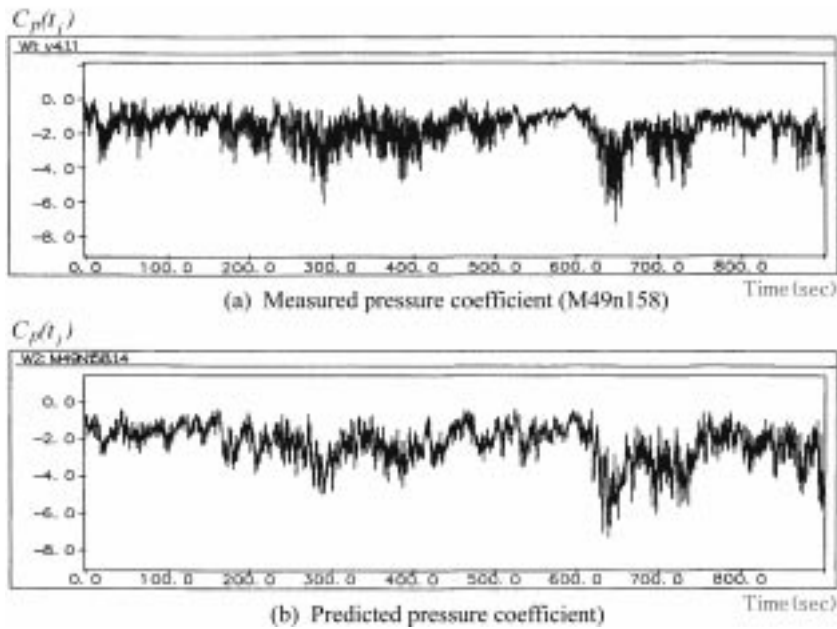


Fig. 16 Comparison of pressure coefficients

gives the calculated instantaneous pressure coefficient  $C_p(\alpha_i)$ . The factor  $[u(t_i) / U]^2$ , accounting for the wind-speed dependence of the instantaneous pressure coefficient  $C_p(t_i)$ , is presented in Fig. 15(d).

Fig. 16 compares the measured pressure coefficient with the predicted one. The comparison is satisfactory, given the simplicity of the model. However, the measured pressure coefficient contains more high-frequency contents. This is possibly because of the spatial variations and temporal fluctuations of the incident wind, since the conical vortex at any instant is comprised of incident airflow entrained into the circulation from different locations along the roof edge, a situation the proposed model cannot accommodate.

Of course, while the incident wind speed and the incident wind angle are the most important parameters affecting the roof-corner pressure, there are other contributing factors. For instance, the vertical profile of the incident wind speed and the height of the building are important in determining how much airflow would go over the roof, thus influencing the vortices and the pressure. The instantaneous incident wind speed profiles are similar, while the wind speeds fluctuate about a certain mean boundary-layer wind profile; it is perhaps this wind-speed-profile similarity that makes the model prediction of pressure possible with reasonable accuracy, using upstream wind measured at a single point (of the wind speed profile). The findings made in this study are significant from the viewpoint of practical applications: fluctuating wind pressure data can be generated from (full-scale measured or computer-simulated) incident wind speed and direction, and the mean pressure coefficients obtained in wind-tunnel tests.

Pressure prediction for tap 50101 is less successful, using the mean pressure coefficient-mean AOA relationship obtained in full-scale testing. Depending on the instantaneous upstream wind direction, the wind flow passing over the tap is either straight (with small cornering vortices) or vortical (with one large vortex formed at one of the edges). Thus, there are two different flows

involved that affect the pressure at this tap, i.e., straight flow and vortical flow. In this particular situation, the pressure coefficient-wind angle relationship required in the prediction model could not be adequately represented by the mean pressure coefficient-mean wind angle relationship obtained in the full-scale testing. This is because in full-scale experiments the wind direction fluctuates significantly during a typical time period of 15-minute data runs, resulting in two types of flow as mentioned earlier that will influence the mean pressure at tap 50101. Better prediction could be achieved if the required pressure coefficient-wind angle relationship is approximated by the mean pressure coefficient-mean wind angle relationship established from wind-tunnel tests where large directional fluctuations do not occur.

## 5. Separation bubble

When wind approaches a building normal to one of its walls, the obstructed flow is forced to go upward over the building, downward along the windward wall and around the wall corners. Woo *et al.* (1977) has given a conceptual model of the flow around a cube. The up-wash flow cannot negotiate the sharp roof edge to remain attached because of the viscosity of the air. Instead, the flow separates to form a shear-layer, which may reattach to the roof surface somewhere downstream to generate a vortical circulation called the separation bubble (SB). This section examines the flow structure in a vertical cross section within the SB and the correlation between the flow structure and the roof pressure distribution. A time-averaged structure of the SB is first established from the measurements of wind flow inside the SB. The mean pressure developed on the roof underneath the SB is then investigated. The concept of a *non-conventional pressure coefficient* is introduced to facilitate the separation of the effect of the wind direction fluctuation from that of the wind speed on the pressure-generating mechanism on the roof under the SB.

### 5.1. Structure of separation bubble

Systematic measurements of the wind flow within the SB were conducted using one sonic anemometer. To measure the flow inside the separation bubble, the sonic anemometer is mounted on a portable, sturdy support, which could be moved to any desired locations. Fig. 2 shows the setup of the sonic anemometer on the roof. Based on the measurements, the mean structure of the SB is established in the form of normalized velocity vectors.

#### 5.1.1. Measurement of flow inside separation bubble

In order to establish the mean structure of the separation bubble in the vertical plane along the short roof axis, more than one hundred data runs of point-measurement of wind velocity inside the SB were conducted; each record was 15 minutes long. The measurement covers the entire length of the short axis and up to 1.27 m (4' - 02'') from the roof surface.

#### 5.1.2. Velocity vectors and boundary of separation bubble

The data-runs are analyzed to yield information about the mean magnitudes and orientations of the velocity vector matrix. The magnitudes are normalized by their corresponding mean wind speeds measured at the roof-height level (4 m or 13 ft) on the meteorological tower. One 15-minute data

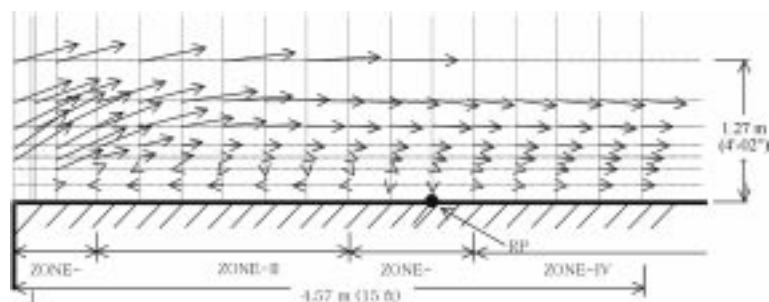


Fig. 17 Mean structure of the SB, as represented by velocity vectors

record is required to obtain one velocity vector. A sketch of the SB created from the computed velocity vectors is presented in Fig. 17. In the plot, the size of the velocity vectors is proportional to the magnitude of the velocity. It is worth mentioning that the data used to create the plot were collected over a time period of several months.

A few observations can be made about the time-averaged SB:

1. The vortex is oblong and elongated in the direction of upstream wind;
2. The mean reattachment point (RP), as identified by a nearly downward-pointing velocity vector, is approximately 3.0 m (10 ft) from the leading edge;
3. The region upstream of the mean reattachment point with predominant flow reversal is confined close to the roof surface; in this region, frequent flow reversal occurs as known from time series traces;
4. In the immediate proximity of the roof, there exist four distinct zones of wind flow (Fig. 17); they are the leading edge zone (ZONE-I), where the separated shear layer meets the reverse flow to create a wedged region, the reverse flow zone (ZONE-II), the reattachment zone (ZONE-III), and the forward flow zone (ZONE-IV); and
5. Despite the random and turbulent nature of the flow inside the SB, the averaged structure of the SB is regular and well organized. This was also confirmed by the flow visualization using the airfoil-grid method (Sarkar *et al.* 1997).

An effort is made to define the boundary of the separation bubble. Sarkar *et al.* (1997) use a parameter called *intermittence factor* (I.F.) to define the boundary of the SB. The *intermittence factor* is defined as the fraction of a certain time interval when the local flow goes in the direction opposite to that of the upstream wind; the time interval used in this study is 15 minutes. The I.F. value is also an indicator of flow turbulence.

The same data used to obtain the velocity vectors in Fig. 17 are analyzed to calculate the I.F. values for the horizontal velocity component along the short roof axis. The boundary of the SB is defined by a curve connecting those measurement points above which there is no flow reversal, starting from the leading roof edge, Fig. 18. The portion of the boundary downstream of the mean reattachment point, as marked by the broken line in Fig. 18, is not definitive due to the limited information available from this full-scale study. Occasional large wind-direction excursions from the perpendicular-to-front-wall direction might have added uncertainty to the evaluation of I.F. values. Wind-tunnel tests under well-controlled wind conditions could possibly give a more precise definition of

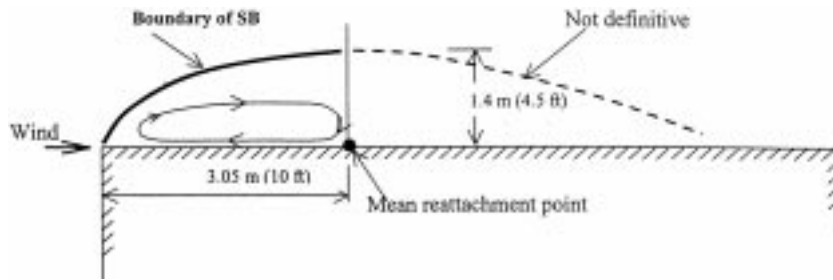


Fig. 18 Boundary of the SB

the boundary downstream of the mean reattachment point.

Notwithstanding the well-organized mean structure of the separation bubble, it is worth pointing out that the flow inside the SB is highly turbulent, as indicated by the I.F. values.

### 5.2. Mean-pressure distribution under separation bubble

Following the discussion of the mean structure of the SB, it is natural to take a close look at the mean pressure distribution on the roof so that the mean structure of the SB and the mean pressure distribution can be correlated.

Averaged mean pressure coefficients for six taps along the short roof-axis were available. These taps are 50123, 50223, 50523, 50923, 51423, 52323 and 52923. The number of mean pressure coefficients used in averaging is about ten.

Since the mean reattachment point (RP) is at about 3 m (10 ft) from the leading edge, taps 50123, 50223, 50523 and 50923 are located upstream of the RP; taps 51423, 52323 and 52923 are downstream of the RP.

A closer look at the velocity vectors near the roof leading edge reveals that taps 50123 and 50223 are in the wedge-shaped region where the separated shear layer meets the reverse flow (Fig. 19). These two taps experience the strongest suction; the air in that wedge-shaped parcel is entrained upward to create a zone of strong suction.

Taps 50523 and 50923 are located within the zone of flow reversal and their mean pressures differ only slightly (Fig. 20). Taps 52323 and 52923 are in the forward flow zone, and the difference in their mean pressures is small. Tap 51423 assumes a mean pressure coefficient falling somewhere in between the values for the two neighboring zones.

Wind-tunnel testing was performed by Lynthe and Surry (1983) to study the wind loading of flat roofs. Due to the difference in plan aspect ratios between the wind-tunnel model and the Texas Tech

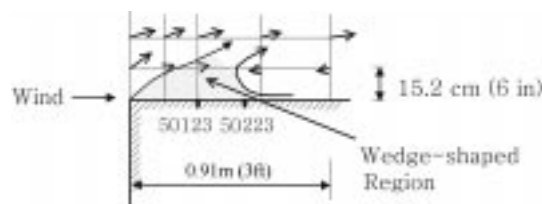


Fig. 19 Wind flow near the leading roof edge

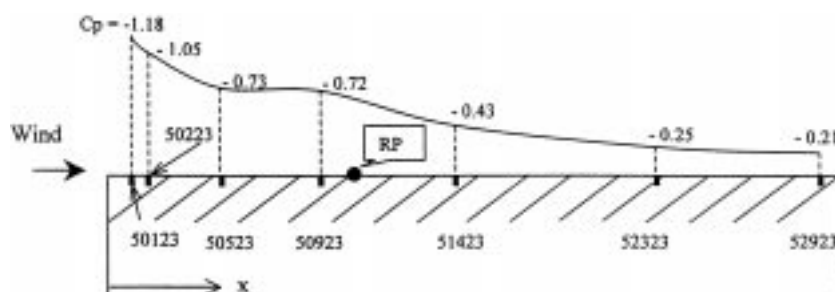


Fig. 20 Distribution of averaged mean pressure underneath the SB

Experimental Building and the difference in the testing wind direction, no direct comparison of pressure distribution between the two is possible. The relative height of the front wall to the longitudinal plan dimension for the Texas Tech Experimental Building is  $13/30 = 0.43$ ; the closest corresponding ratios used in the wind tunnel test were  $100/400 = 0.25$  and  $200/400 = 0.5$ . Pressure data at the edge of the full-scale test building was not available; therefore, it is not known whether the pressure will increase or decrease upstream of Tap 50123. Lythe and Surry (1983) found that the pressure distribution becomes more uniform and the maximum suction moves downstream as the relative height increases.

### 5.3. Mechanism of peak-pressure generation

To better understand the mechanism of peak-pressure generation on the roof under the SB, i.e., the cause-effect relationship between the incident wind and the induced pressure, a few runs were subjected to detailed analysis. These data consist of simultaneously recorded time series of the incident wind speed, the incident wind direction and the pressure coefficients. In the experimental setup, sonic anemometer #2 was placed above the leading edge to measure the incident wind as it approached the building. Specifically, time series of pressure coefficient for tap 50223 is examined and correlated with synchronized time series of the incident wind speed and direction. The pressure measured at tap 50223 responded to the fluctuation of the incident wind with negligibly small time lags.

#### 5.3.1. Some observations on incident wind speed and direction fluctuation

Natural wind changes its direction and speed constantly. Full-scale data by the sonic anemometers indicate that a typical range of wind direction fluctuation is around  $80^\circ$  in a time period of 15 minutes. Besides, large fluctuations can occur in a very short time period. Wind direction fluctuations in the order of  $60^\circ$  were observed to happen in one tenth of a second [Fig. 21(a)]. Propeller-type anemometers such as the UVW-type would have failed to detect such fast fluctuations of the wind direction. The variation of wind speed in a typical 15-minute run is also significant, but at much slower rates than that of the wind direction [Fig. 21(b)]. Both the wind-direction fluctuation and the wind-speed variation are important in the pressure-generation process. It seems that fluctuations of wind speed and wind direction are not entirely independent. Large-and-fast fluctuations of the wind direction are often accompanied by a drop in the wind speed (Fig. 21).

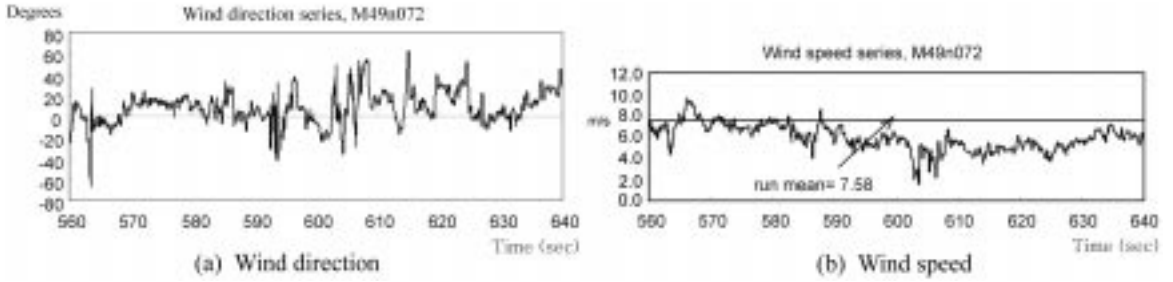


Fig. 21 Fluctuations of incident wind

### 5.3.2. Concept of non-conventional pressure coefficient

Pressure coefficients [ $C_p(t)$ ] typically used are obtained by normalizing the pressure [ $p(t)$ ] by a time-averaged free-stream dynamic pressure measured at a reference height. That is,

$$C_p(t) = p(t) / (\rho V^2 / 2) \quad (1)$$

In Eq. (1),  $p(t)$  is the instantaneous pressure,  $\rho$  is the air density and  $V$  is an averaged wind speed over a time period. Again, this widely-used definition is practically convenient but not necessarily consistent in the sense that  $C_p(t)$  calculated in this way is not unique, although  $p(t)$  is. The  $C_p(t)$  defined in Eq. (1) is not only dependent on  $p(t)$ , which is unique, but also dependent on the wind speed fluctuations in the entire period over which the averaging is performed to compute  $V$ . The statistics of pressure coefficients defined in Eq. (1) would be different, given the same pressure data, had a different time interval and starting point been used. Understandably, a shorter duration yields higher averaged-wind speeds and therefore lower pressure coefficients.

As depicted in Fig. 22(b), there is a period of 50 seconds (640~690 s) in which the conventional  $C_p(t)$  takes on relatively small values (low suctions) simply because of the lower-than-the-average incident wind speed during that time interval. In the same record, the higher-than-average  $C_p(t)$  is mostly a result of wind gust [695 ~ 715 s, Figs. 22(b) and 22(d)]. Although the pressure  $p(t)$  can be recovered from the  $C_p(t)$  values for a given mean wind speed, the conventional pressure coefficient is misleading and is not consistent with the fact that the pressure coefficient should be wind-speed independent. The concept of a *non-conventional* pressure coefficient is introduced here to define a pressure coefficient that is truly wind speed independent.

To obtain the *non-conventional* pressure coefficient,  $\widehat{C}_p(t)$ , an instantaneous dynamic pressure is used for normalization, instead of a time-averaged or run-averaged dynamic pressure.

The non-conventional pressure coefficient is defined as:

$$\widehat{C}_p(t) = p(t) / (\rho v^2(t) / 2) \quad (2)$$

This definition is consistent in the sense that both the numerator and the denominator are fixed values at  $t$  and are not dependent on their corresponding fluctuations before and after the instant  $t$ . In this definition, instead of the averaged dynamic wind pressure that changes with the duration and

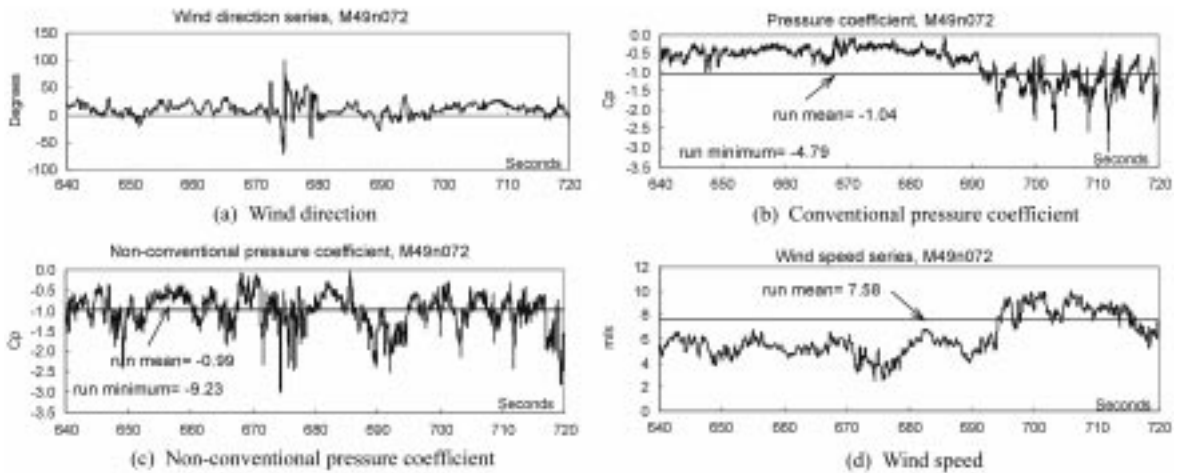


Fig. 22 Simultaneous traces of incident wind and pressures (M49n072, 640 s ~ 720 s)

starting point of averaging, an instantaneous dynamic wind pressure is used for normalization. The defined pressure coefficient is thus unique. The instantaneous dynamic pressure used in this discussion is calculated by using the incident wind speed measured with sonic anemometer #2 placed right above the leading edge. The sonic wind speeds are corrected by the correction factors listed in Table 2 to reduce them to the undisturbed upstream wind speeds at the same level. The introduction of the *non-conventional* pressure coefficient eliminates the dependence of the pressure coefficients on the mean wind speed; thus, the role of the wind-direction fluctuations in the pressure-generating process can be studied separately. The *non-conventional* pressure coefficient,  $\hat{C}_p(t)$ , reflects the pressure-generating mechanism governed by parameters other than the magnitude of the incident wind-speed, such as the upstream wind profile, the incident wind-direction fluctuations and the wind-structure interaction.

### 5.3.3. High suction and wind-direction fluctuation

A cause-effect relationship between the incident wind and the pressure coefficient is of interest. However, pressure coefficient data indicate that the mean and the minimum pressure coefficients of tap 50223 at wind angles around  $270^\circ$  are not sensitive to the AOA *per se*, as is shown in Fig. 23. This suggests that factors other than the wind direction are responsible for high suction on the roof surface. In other words, the wind direction by itself does not induce high suction.

The directional *fluctuation* (not the direction itself) seems to be the most important single input to the incident wind-pressure relationship; other contributing factors such as the wind speed profile are put aside to simplify the situation. Fig. 24 displays four synchronized segments of 80-second duration for the incident wind direction, the conventional pressure coefficient, the non-conventional pressure coefficient, and the wind speed. A close comparison of the directional fluctuations (Fig. 24(a)) with the trace of the non-conventional pressure coefficient (Fig. 24(c)) reveals that the primary peaks of  $\hat{C}_p(t)$  coincide with the large-and-fast fluctuations of the wind direction. It is difficult at this stage to quantify the effect of the directional fluctuations. Qualitatively, it can be said that the way the direction fluctuates, e.g., the short-term mean direction about which the direction fluctuates and the

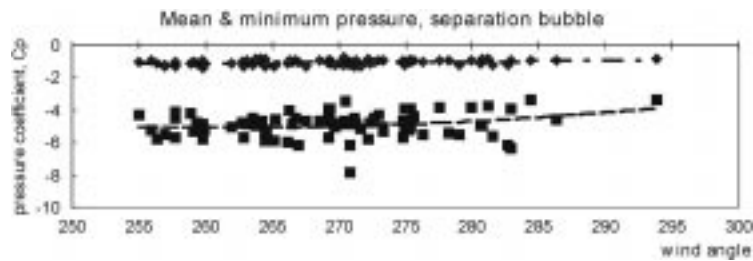


Fig. 23 Pressure coefficient versus wind angle (tap 50223)

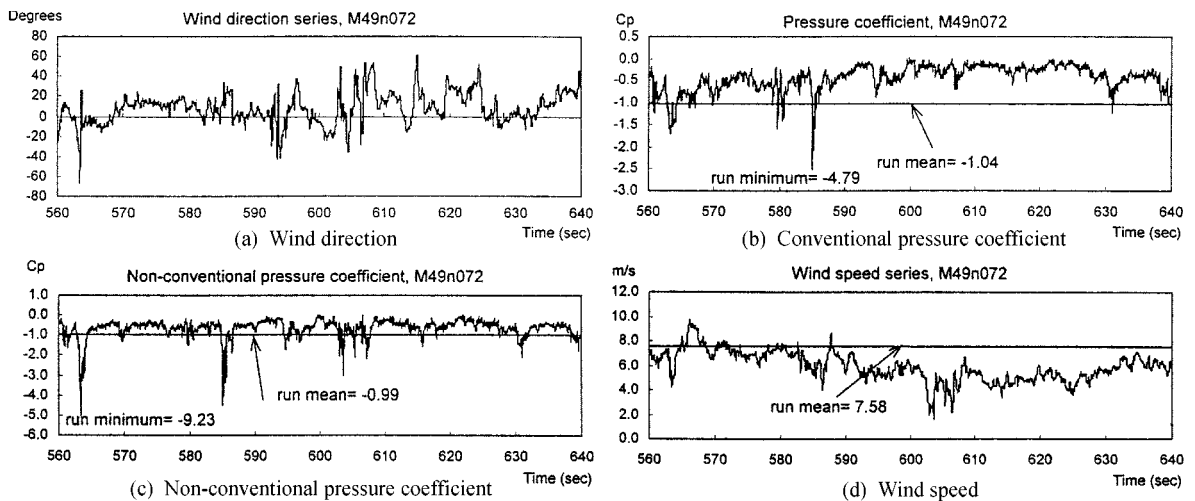


Fig. 24 Simultaneous traces of incident wind and pressures (M49n072, 560 s ~ 640 s)

rate of fluctuation, are factors governing the  $\widehat{C}_p(t)$ . Further research is needed to quantify the effects of the wind direction fluctuations. A possible explanation for this observation follows.

The SB is considered a two-dimensional phenomenon; it takes some time for a balance to establish within the SB. Fluctuations of incident wind direction disturb the delicate balance. A large-and-fast wind direction fluctuation around  $270^\circ$  AOA preceded by a mostly steady wind direction seems to break this balance to initiate high suction.

Observations indicate that the primary peaks of the conventional pressure coefficient in the SB are often an outcome of combined large-and-fast *fluctuations* of the incident wind direction and wind gusts, with the former playing a more important role [Figs. 24(b) and 24(c)]. Slow (but not necessarily small) fluctuations of the incident wind direction only induce weak suction [small-magnitude  $\widehat{C}_p(t)$ ], see the segments from 564 second to 580 second in Figs. 24(a) and 24(c).

It is unclear at this point what is happening to the wind flow inside the SB at instants of high suction. Simultaneous, multiple-point velocity measurements are desirable for an affirmative answer. Letchford (1995) claimed that some shear-layer instability, which is strongly influenced by the incident turbulence, is an important parameter in this respect; he postulated that some instability caused by incident turbulence forces the separated shear layer to prematurely reattach onto the roof, creating

peak suctions.

An effort is also made in this study to establish certain airflow patterns of the SB associated with high suctions, using the conditional sampling technique adopted by Marwood (1996) for the conical vortex situation. No simple and clear pattern emerged, except it was observed that the airflow inside the SB at moments of high suctions was quite three-dimensional. The flow inside the SB seemed to defy a two-dimensional characterization at instants when high suctions are induced on the roof surface. More work is needed for the quantification of the SB airflow-roof pressure relationship. However, the current study suggests an answer to the question posed by Letchford (1995) as to the cause of shear-layer instability: large-and-fast directional fluctuations of the incident wind might be the initiator of the shear-layer instability, which he believed was the cause of high suctions. Tieleman (1992) has emphasized the importance of properly simulating the lateral turbulence or the direction fluctuations for improved reproduction of peak pressures in wind-tunnel model tests.

## **6. Conclusions**

The major points discussed about the cornering vortices can be summarized as follows.

1. In terms of the relationship between the roof-corner pressure and the airflow within the conical vortices, a fundamental concept is that low pressures (high suctions) are always related to strong vortical circulation;
2. The vortices and the vortex-pair patterns vary considerably with the incident wind angle; the pressures on the roof corner react closely to the fluctuations of the incident wind speed and direction;
3. Wind angles favoring vortex formation are approximately bounded between  $200^\circ$  and  $250^\circ$  AOA, a 50-degree range symmetrical about the roof-corner bisector; and
4. Instantaneous pressure coefficients for tap 50501 could be satisfactorily predicted from the mean pressure coefficient-mean wind angle relationship and the incident wind direction and speed information. Pressure prediction for tap 50101 was less successful; better prediction is expected if wind tunnel data of the mean pressure coefficient as a function of mean wind angle are used instead of the full-scale data.

The major observations for the separation bubble case are:

1. The overall SB is oblong and elongated; four flow zones near the roof surface can be identified: (a) the leading-edge zone, where the separated shear-layer meets the reverse flow to create a wedge-shaped region; (b) the reverse-flow zone; (c) the reattachment zone; and (d) the forwarding-flow zone;
2. The location of the mean point of reattachment is approximately 3.0 m (10 ft) from the leading roof edge; the mean height of the SB is about 1.4 m (4.5 ft);
3. The mean pressure distribution on the roof surface is directly related to the structure of the SB; the suctions on the roof generally decrease with distance from the leading edge;
4. The introduction of the non-conventional pressure coefficient made it possible to separately investigate the effects of wind speed and the wind direction on pressure generation;
5. Time series analyses indicate that large-and-fast fluctuations of the incident wind direction govern the mechanism of peak-pressure generation;
6. The primary peaks of the conventional pressure coefficient are often a result of combined wind-direction fluctuations and wind gusts; and

7. The incident wind affects two types of pressure quantities: *single event*, such as the peak pressure, and *statistics*, such as the mean and the rms pressures. The turbulence intensities, reflecting the gust structure and the directional fluctuations of the incident wind, might collectively bear significant influences on the pressure *statistics*. The peak-pressure coefficient associated with the SB seems to be governed by the lateral directional fluctuations of the incident wind. More research is clearly needed to better understand the effects of the incident wind directional fluctuations.

## Acknowledgements

This study is the outcome of one of the four research areas pursued under the Colorado State University/Texas Tech University Cooperative Program in Wind Engineering that is sponsored by the US National Science Foundation (NSF). The authors acknowledge the financial support provided by NSF under Grant # 9409869.

## References

- Banks, D., Meroney, R.N., Sarkar, P.P., Zhao, Z. and Wu, W. (2000), "Flow visualization of conical vortices on flat roofs with simultaneous surface pressure measurement", *J. Wind Eng. Ind. Aerod.*, **84**, 65-85.
- Hoxey, R. and Short, L. (1999), "Quasi-steady theory developed with experimental verification", *Proc. the 10th Int. Conf. on Wind Eng.*, 1679-1686, Copenhagen, Denmark.
- Kawai, H. and Nishimura, G. (1996), "Characteristics of fluctuating suction and conical vortices on a flat roof in oblique flow", *J. Wind Eng. Ind. Aerod.*, **60**, 211-225.
- Letchford, C.W., Iverson, R.E. and McDonald, J.R. (1993), "The application of the quasi-steady theory to full-scale measurements on the Texas Tech Building", *J. Wind Eng. Ind. Aerod.*, **48**, 111-132.
- Letchford, C.W. (1995), "Simultaneous flow visualization and pressure measurements on the Texas Tech Building", *Proc. the 9th Int. Conf. Wind Eng.*, 524-535, New Delhi, India.
- Lynthe, G. and Surry, D. (1983), "Wind loading of flat roofs with and without parapets", *J. Wind Eng. Ind. Aerod.*, **11**, 75-94.
- Marwood, R. (1996), "An investigation of conical roof edge vortices", Ph.D. dissertation, Lincoln College, University of Oxford.
- Sarkar, P.P., Zhao, Z. and Mehta, K.C. (1997), "Flow visualization and measurement on the roof of the Texas Tech Building", *J. Wind Eng. Ind. Aerod.*, **69-71**, 597-606.
- Tieleman, H.W. (1992), "Problems associated with flow modeling procedures for low-rise structures", *J. Wind Eng. Ind. Aerod.*, **41-22**, 923-934.
- Tieleman, H.W., Surry, D. and Lin, J.X. (1994), "Characteristics of mean and fluctuating pressure coefficients under corner (delta wing) vortices", *J. Wind Eng. Ind. Aerod.*, **52**, 263-275.
- Woo, H.G.G., Peterka, J.A. and Cermak J.E. (1977), "Wind-tunnel measurements in the wakes of structures", NASA Contractor Report NASA CR-2806, National Aeronautics and Space Administration.
- Zhao, Z. (1997), "Wind flow characteristics and their effects on low-rise buildings", Ph.D. dissertation, Department of Civil Engineering, Texas Tech University.

AK